J Mater Sci (2010) 45:1255–1263
DOI 10.1007/s10853-009-4076-5

# Mesoporous titania–silica composite from sodium silicate and titanium oxychloride. Part I: grafting method

**Askwar Hilonga · Jong-Kil Kim · Pradip B. Sarawade · Hee Taik Kim**

Received: 22 September 2009 / Accepted: 24 November 2009 / Published online: 5 December 2009


**Abstract** In this study, we report a versatile method for designing a titania–silica composite using relatively inexpensive precursors. The composite was synthesized by grafting (impregnating) a precursor of a guest component into the preformed host's solid network. The latter was prepared using sodium silicate as a silica precursor in the presence of cetyltrimethylammonium bromide (CTAB). A freshly prepared solution of titanium oxychloride ($TiOCl_2$, titania precursor that is relatively stable) was introduced into the host's network to develop a titania–silica composite with initial ratio of Ti:Si = 1. The final product has the overall ratio of Ti:Si = 7:3 and was obtained after calcination for 5 h at 600–1000 °C. The XRD patterns for the calcined samples indicate the presence of $TiO_2$, and there was a significant increase in peak intensity as the calcination temperature increased. EDS, XRF, and FT-IR analyses indicated the formation of a highly pure composite rich in Ti, Si, and O. A Si–O–Ti band at 954 $cm^{-1}$ was observed, confirming the formation of a titania–silica composite. A composite with optimum properties (homogenous dispersion of the composite and less individual oxide phase separation) was obtained at 600 °C. A similar experiment was also conducted in the absence of CTAB. In this case, the final product was microporous, rendering it unsuitable for some applications.

**Electronic supplementary material** The online version of this article (doi:10.1007/s10853-009-4076-5) contains supplementary material, which is available to authorized users.

A. Hilonga · P. B. Sarawade · H. T. Kim (✉)
Department of Chemical Engineering, Hanyang University, 1271 Sa 3-dong, Sangnok-gu, Ansan-si, Gyeonggi-do 426-791, Republic of Korea
e-mail: khtaik@yahoo.com; khtaik@hanyang.ac.kr

J.-K. Kim
E&B Nanotech. Co., Ltd., Ansan-si, Gyeonggi-do, Republic of Korea

## Introduction

Mesoporous materials have attracted much interest since the early 1990s. Many potential applications have been explored from catalysis, environmental monitoring, and pharmaceuticals to clinical toxicology, but a gap in real industrial applications still exists [1]. Some of the applications of mesoporous materials involve the innovative use of $TiO_2$ particles, as these particles have large specific surface areas and high catalytic performance. The efficiency of $TiO_2$ is influenced by several factors, such as its crystalline structure [1], particle size [2], and preparation methods [3]. $TiO_2$ particles are small in size, and therefore difficult to separate and recover from the reaction mixture. $TiO_2$ can be grafted into a silica network to form a titania–silica composite [4–7]. These composites have aroused considerable interest due to their use as thin paper fillers [8] and in the photodegradation of organic pollutants [9]. This type of composite has also been reported to have high thermal stability and chemical durability [6].

Conventional composite material synthesis is based on three primary techniques: (1) incorporating the guest component into the silica ($SiO_2$) structure when the composite is formed [10]; (2) grafting precursors of the selected guest components into the preformed host's solid network, in which the precursors react to form active centers [11]; and (3) using silica as a template for the guest components for synthesizing materials with new crystalline structures [12]. Materials prepared by grafting precursors of the selected guest components into the preformed host's solid network (post-functionalization) have been reported to

have improved physical–chemical properties [13]. Several publications have also reported that titania–silica composites show desirable properties [14–16], the most important one being good preservation of the mesostructure. However, the performance of the composite is affected by phase transformation and loss of surface area at higher temperatures, low titanium loading, and deterioration of the framework order [17, 18]. To realize the full potential of this type of material, it is necessary to manufacture composites from relatively inexpensive precursor materials and to ensure that certain desirable characters (for thin paper filler [8] and catalysis [14–16]), including large porosity, narrow pore size distribution, high thermal stability, and homogeneous dispersion of the composite, are features of the composite produced.

Most of the reported methods for gel formation are based on the catalytic hydrolysis and polycondensation of tetraethoxysilane (TEOS) [19–21]. To the best of our knowledge, few studies have reported using sodium silicate as a silica precursor for synthesizing titania–silica composites with desirable properties. Although the existing literature provides some useful information on the use of sodium silicate as a silica precursor [22 and references therein], additional research is required to develop composites with more desirable properties, because existing studies that used sodium silicate as a precursor have several limitations such as low temperature anatase–rutile phase transformation, lower BET surface area, emphasis on silica content (while overlooking the influence of calcination temperature), and failure to develop materials with suitable porosity (in some cases). We anticipate that a systematic investigation into methods to produce titania–silica composites with desirable properties based on an inexpensive silica precursor (sodium silicate) will increase the utility of this type of composite and negate the requirement for the relatively expensive silica precursors that are currently used. Moreover, the use of titanium oxychloride (which has been rarely reported [23, 24]) facilitates the formation of a final product that has desirable properties such as high-purity, an even distribution, and high loading of titania in the composite (probably due to its rapid reaction with silanols and efficient polymerization during the network formation). It is also a relatively stable form of titania precursor which reacts with silica precursor even at lower temperatures (40–60 °C). It should be noted that other titania precursors such as titanium butoxide [$(Ti(OBu)_4$] can only be homogenously dispersed in silica matrix when $Si/Ti \geq 10$ [25] and in some cases a long hydrothermal treatment time is required for tetrapropylorthotitanate (TPOT) to produce a final product with high titania loading [26].

As part of our continuous research program to develop titania–silica composites with more desirable properties for various applications, such as photodegradation of organic pollutants and as a thin paper filler, we have developed a controllable and reproducible method to produce composite titania–silicate aggregates with high thermal stability, optimum porosity, and high BET surface area using a relatively inexpensive silica precursor.

## Experimental procedures

### Materials

Sodium silicate (24% $SiO_2$, 7.4% $Na_2O$) was purchased from Shinwoo Materials Co. Ltd., Republic of Korea. Ammonia solution (28% $NH_3$), hydrochloric acid (36% HCl), titanium tetrachloride ($TiCl_4$), and cetyltrimethylammonium bromide (98+% CTAB) were purchased from Duksan Chemicals, Republic of Korea.

### Preparation of $TiOCl_2$

The aqueous solution of $TiOCl_2$ was prepared as described previously [8]. In short, 16.5 mL of reagent grade $TiCl_4$ was dropped slowly into a three-neck flask (in an ice bath) containing 33.5 mL of distilled water. Then, three drops of 1 M HCl was added to prevent hydrolysis and precipitation. The product obtained was labeled as the $TiOCl_2$ stock solution. Because $TiOCl_2$ was prepared at a temperature below room temperature and used immediately, all Ti atoms were in monomeric form (FT-IR analysis did not show the vibration bands associated with the presence of –Ti–O–Ti– polymer) and no precipitates were observed.

### Preparation of pure silica support

To develop a solid support with controllable and reproducible porosities, a fixed amount of CTAB was used as a template under well-controlled reaction conditions. The experiment was performed as follows: 3 g of CTAB was dissolved in 30 mL of 2 N HCl solution at room temperature with stirring. After 10 min, 4 g of sodium silicate was added. The sodium silicate was first hydrolyzed for 10 min in this strongly acidic solution. When sodium silicate is hydrolyzed by HCl, silicic acid and NaCl are generated. The $Na^+$ and $CTA^+$ act as flocculating agents, as described later in this article ("Results" and "Discussion" section). Five milliliters of ammonia solution (28%) was then slowly added after 1 h to induce gelation, and the final gel was aged for 2 h. The as-synthesized materials were rinsed with water and dried at 110 °C for 2 h. The product obtained was called pure silica (PS). The as-synthesized sample was specifically denoted PS-Asyn. This experimental procedure was repeated in order to prepare each of the samples that

**Table 1** BET surface area, pore size, and pore volume of the prepared materials at various calcination temperatures (As-synthesized (Asyn), 600, 900, and 1,000 °C)

| Sample | Calcination temp. (°C) | BET surface area ($m^2$/g) | Pore diameter (Å) | Pore volume ($cm^3$/g) |
|---|---|---|---|---|
| PS-1 | Asyn | 245 | 32.4 | 0.50 |
| PS-2 | 600 | 529 | 34.1 | 0.79 |
| PS-3 | 900 | 465 | 33.3 | 0.65 |
| PS-4 | 1000 | 410 | 33.0 | 0.61 |
| TSC-1 | Asyn | 253 | 33.9 | 0.38 |
| TSC-2 | 600 | 340 | 36.0 | 0.41 |
| TSC-3 | 900 | 202 | 34.8 | 0.30 |
| TSC-4 | 1000 | 231 | 32.6 | 0.39 |

were subsequently calcined at the range of 600–1,000 °C for 5 h. These samples were denoted as PS-2, PS-3, etc., as summarized in Table 1.

It should be noted that one of the main advantages of using TEOS as a silica precursor is that all byproducts are volatile, as they are usually alcohols. However, because the precursor employed in the present study may leave residues (such as $Na^+$ and $Cl^-$) behind in the structure and consequently alter the properties of the material, the as-synthesized materials were first thoroughly washed with water and then rinsed with ethanol. By following this procedure, all byproducts were successfully removed as assessed using an instrument that can measure the ions of sodium and chlorine (pH/ISEK Meter pH-250L, Korea). The purity of the final product was also confirmed by EDS and XRF; the only elements present in the composite were Ti, Si, and O.

## Reaction of $TiOCl_2$ with the silica support

A titania–silica composite was prepared by impregnating titanium oxychloride (guest) into a preformed solid silica network (host) at Ti:Si = 1. Thus, the entire PS (host) sample obtained, as explained in section "Preparation of pure silica support", was immersed in 10 mL of water at 50 °C. Then, 10 mL of $TiOCl_2$ (guest) was added slowly and stirred for 10 min before adding 30 mL of water. The reaction was continued for 2 h under well-controlled conditions. The solids were then filtered and washed with ethanol and dried at 110 °C for 2 h and then re-calcined. These experimental procedures were done for each of the samples prepared in section "Preparation of pure silica support". The final products are referred to as titania–silica composites (TSC) and denoted as TSC-1, TSC-2, etc., depending on their respective calcination temperature. To evaluate the influence of CTAB on the porosity of the composite, a similar experiment was conducted in the absence of CTAB (untemplated titania–silica composite). The results obtained for this product are discussed briefly under the section "Nitrogen physisorption studies". The experimental procedures reported in this work were repeated three times to examine the reproducibility of the properties of the final products. Generally, there were no significant differences between the properties of the products obtained from the three batches.

## Characterization

The morphologies of the titania–silica composite samples were characterized using an scanning electron microscope (FE-SEM, Hitachi, S-4800) with an accelerating voltage of 15 kV. Before FE-SEM characterization, samples were dried at 110 °C and sprinkled lightly using a spatula onto carbon tape with an adhesive surface that was affixed to an aluminum stub. The stub was placed into a sputter coater and a thin layer of gold was applied to the surface for 5 min. The FE-SEM was coupled to an energy dispersive spectroscope (EDS with a detection limit of 100 ppm and depth resolution up to 3 μm) to assess the purity and elemental composition of the final product. A transmission electron microscope (TEM) micrograph was obtained using a JOEL 2000FX instrument. X-ray diffraction patterns (XRD-6000, Shimadzu) were used to determine the crystallinity of the composite. The accelerating voltage and applied current were 40 kV and 100 mA, respectively. The average crystallite size, $D$, was calculated using the Debye–Scherrer formula $D = K\lambda/(\beta\cos\theta)$, where $K$ is the Scherrer constant, 0.9; $\lambda$ is the X-ray wavelength, 1.5406 Å; $\beta$ is the full width at half-maximum (FWHM) of the diffraction peaks, rad; and $\theta$ is the Bragg diffraction angle [27].

The Brunauer–Emmett–Teller (BET) surface areas and porosities of the samples were studied with a nitrogen adsorption instrument (Micrometrics ASAP 2020). All measured samples were degassed at 250 °C for 1 h prior to the measurements. Pore size distribution (PSD) and specific desorption pore volume were determined by the Barrett–Joyner–Halenda (BJH) method. Both adsorption and desorption branches were used to determine PSD. Thermogravimetric analysis (TGA) was performed using a microprocessor-based Parr temperature controller (Model

4846) connected to a muffle furnace (A.H.JEON Industrial Co. Ltd., Korea) at a heating rate of 10 °C/min from room temperature to 1,000 °C. The formation of Ti–O–Si bonds in the prepared composite was confirmed using an AVATAR 360 FT-IR (Thermo nicolet). The X-ray fluorescence of the bulk samples was determined using an XRF-6000 instrument from Shimadzu (with a detection limit of 10 ppm and depth resolution up to 10 μm). ZAF corrections (atomic number ($Z$)) were used to determine the molar ratios of the elements present in the composites.

## Results

### FE-SEM and TEM micrographs

Figures 1 and 2 show representative FE-SEM and TEM micrographs of TSC before and after calcination, respectively. The TSC-1 sample contains primary particles that undergo a finger-like growth pattern, indicated in Fig. 1. The composite "fingers" were as long as 100 nm. At higher calcination temperatures (900 and 1,000 °C), however, the composite (TSC-2) showed significant loss of its finger-like structures (Fig. 2), though up to 900 °C, most of the desirable properties (BET surface area, mesoporosity, homogeneity of $TiO_2$–$SiO_2$) were maintained.

### EDS and XRF analyses

The qualitative composite content was examined using EDS and XRF techniques. Well-resolved, typical signals for oxide, silicon, and titanium were observed (Fig. 2). As anticipated, the characteristic peaks for O, Si, and Ti appeared in the EDS spectrum recorded from a portion of the TSC sample. The EDS results indicate that Ti is incorporated into the TSC when titanium oxychloride is used as a Ti source. The result obtained using EDS were highly congruent with those obtained using XRF, as shown in Table 2 and in the supporting information.

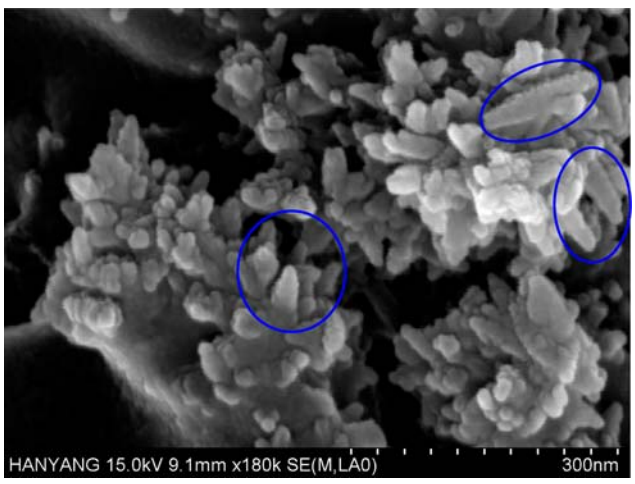


**Fig. 1** The representative FE-SEM micrograph of the as-synthesized sample (TSC-1). The *encircled* regions demonstrate finger-like structures

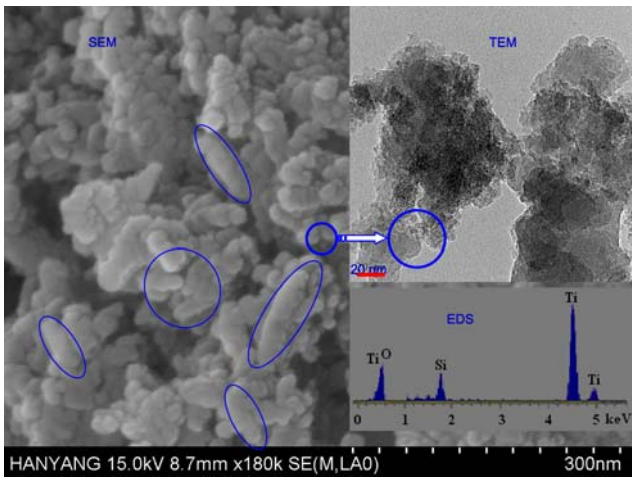


**Fig. 2** The representative FE-SEM micrograph of the calcined sample (TSC-2). The *encircled* regions demonstrate the finger-like structures remnants. The *insets* show TEM micrograph and EDS spectra

### Nitrogen physisorption studies

The representative nitrogen adsorption–desorption isotherms of the PS and TSC samples are shown in Figs. 3 and 4. Generally, the PS and TSC samples exhibited characteristic type IV curves with capillary condensation steps that signify the presence of mesopores. The hystereses loops are very close to the H1 type, according to the IUPAC classification [28], suggesting uniform, cylindrical pore geometry. The average pore size distributions of the PS and TSC samples are presented in Figs. 3 and 4 (insets), respectively. The $P/P_0$ position of reflection points shows that the pore diameter is in the mesopore range, while the narrow hysteresis loop indicates the presence of ordered mesopores. A typical/representative adsorption–desorption isotherm for the untemplated titania–silica composite is presented in Fig. 5. The untemplated titania–silica composite was characterized by type-I adsorption isotherms, which are thought to indicate the presence of micropores [28]. Figure 5 (inset) shows the pore size distributions measured by the BJH method. Generally, the porosity of the final product was less than that of the templated samples.

### XRD patterns

Figure 6 shows the XRD patterns of the as-synthesized titania–silica composite as well as composites that were

**Table 2** Percentages of Si and Ti in TSC calcined at various temperatures (results obtained using EDS and XRF techniques)

| Sample | Calcination temp. (°C) | Si-EDS (%) | Si-XRF (%) | Ti-EDS (%) | Ti-XRF (%) |
|---|---|---|---|---|---|
| TSC-1 | Asyn | 33.5 | 30 | 66.5 | 70 |
| TSC-2 | 600 | 32.6 | 32.1 | 67.4 | 67.9 |
| TSC-3 | 900 | 40 | 30.65 | 60 | 69.35 |
| TSC-4 | 1000 | 25 | 30.2 | 75 | 69.8 |

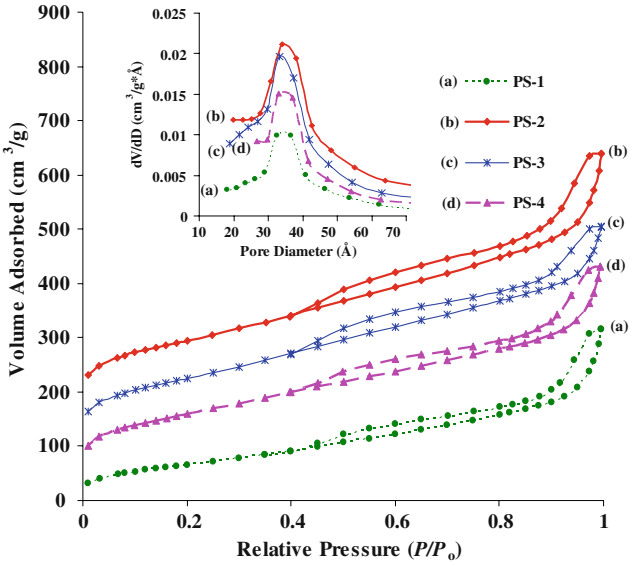


**Fig. 3** Nitrogen adsorption–desorption isotherms and PSD (*inset*) of the PS samples [(*a*) PS-1 (as-synthesized), (*b*) PS-2 (calcined at 600 °C), (*c*) PS-3 (calcined at 900 °C), and (*d*) PS-4 (calcined at 1,000 °C)]. To improve the clarity (to separate them), the isotherms and PSD curves have been offset by a constant specific volume and d*V*/d*D* of 50 $cm^3/g$ and 0.0005 $cm^3/g$ Å, respectively

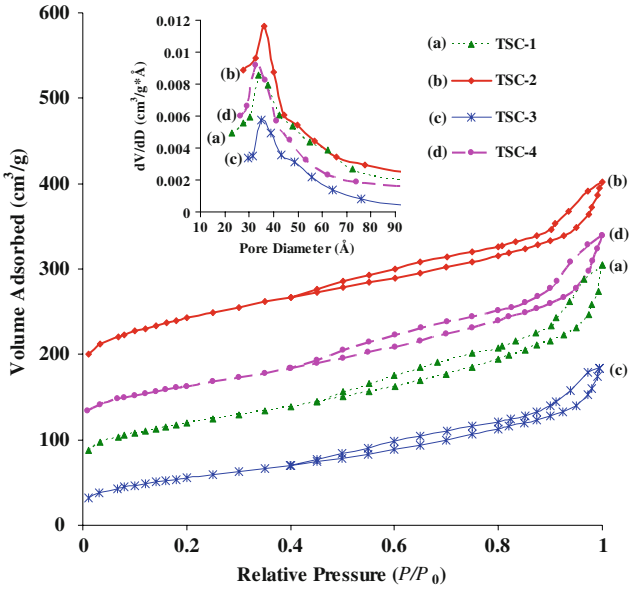


**Fig. 4** Nitrogen adsorption–desorption isotherms and PSD (*inset*) of the TSC samples [(*a*) TSC-1 (as-synthesized), (*b*) TSC-2 (calcined at 600 °C), (*c*) TSC-3 (calcined at 900 °C), and (*d*) TSC-4 (calcined at 1,000 °C)]. To improve the clarity (to separate them), the isotherms and PSD curves have been offset by a constant specific volume and d*V*/d*D* of 50 $cm^3/g$ and 0.0005 $cm^3/g$ Å, respectively

calcined at various temperatures. It is evident that anatase phase $TiO_2$ exists at the lower calcination temperature (600 °C). The diffraction intensities were almost similar up to 900 °C. The average size of the anatase nanocrystals was determined from the full width at half maximum (FWHM) of the anatase (101) peak according to Scherrer's formula [27], and was found to be 13 nm. The low-angle XRD patterns of PS and TSC materials show a reflection in the small-angle region near 2 theta degree = 2.5 (inset in Fig. 6), which indicate the presence of a mesoporous structure. Only one broad diffraction peak (1 0 0) appeared and no other diffraction peaks (such as 1 1 0, 2 0 0, or 2 1 0) were observed, suggesting the lack of a long-range ordered structure [29]. This is in agreement with the nitrogen physisorption studies and the TEM result.

## TGA/DTGA curves

TGA and DTGA (inset) curves of TSC are shown in the supporting information. The DTGA curve shows a broad

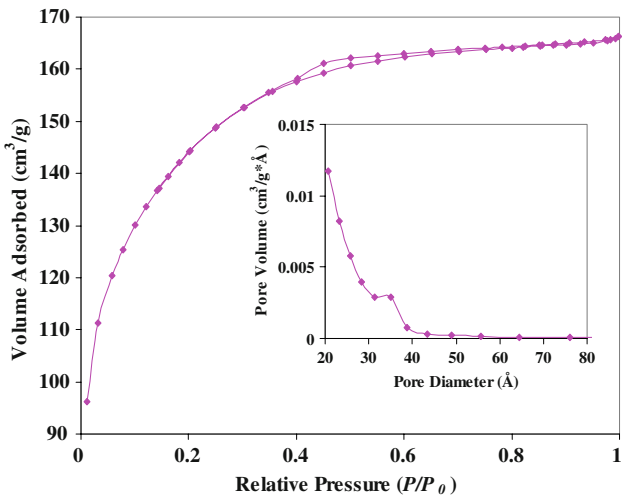


**Fig. 5** Nitrogen adsorption–desorption isotherms of the un-templated sample (without CTAB). The *inset* shows PSD

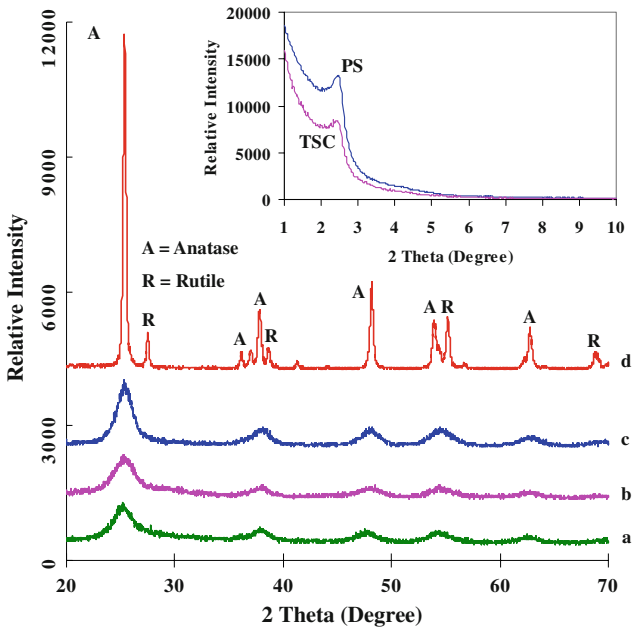


**Fig. 6** XRD spectra of (*a*) as-synthesized titania–silica composite as well as the samples calcined at (*b*) 600 °C, (*c*) 900°C, and (*d*) 1,000°C. The *inset* shows low-angle XRD of PS and TSC

endothermic peak below 100 °C, associated with the evaporation of physically absorbed water. The second significant weight loss observed at 300 °C may be the result of the combustion of a large amount of organic residues. The weight loss observed at 400 °C is probably due to desorption of surface hydroxy groups.

## FT-IR spectroscopy

FT-IR spectra of TSC-1 and TSC-2 samples are shown in Fig. 7. In both spectra, the bands at about 3,450 and 1,640 $cm^{-1}$ can be attributed to the stretching vibrations of

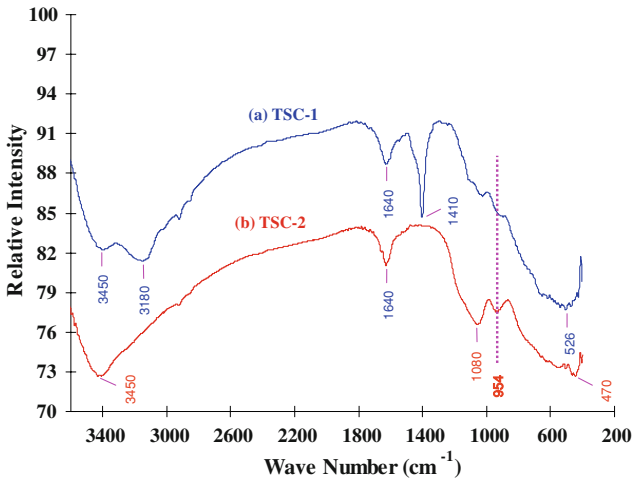


**Fig. 7** FT-IR spectra of (*a*) TSC-1 and (*b*) TSC-2

hydroxyl groups and water, respectively. Moreover, silanol bonds showed absorption at 1,410 $cm^{-1}$. The band at 1,080 $cm^{-1}$ is the asymmetrical vibration of the Si–O–Si bond in the tetrahedral $SiO_4$ unit of the $SiO_2$ matrix [30]. Silica and titania atoms in the composite were connected by Ti–O–Si bonds, as evidenced by the vibration band at 954 $cm^{-1}$. The overall spectra of TSC-2 and TSC-1 samples were largely similar.

## Discussion

The major advantages of the synthesis method proposed in this study (grafting method) are its ability to preserve the mesostructure of the final product (as evidenced using nitrogen physisorption studies, low-angle XRD, and TEM result) and the ability to obtain higher titania loadings (as depicted in Table 2; EDS and XRF results). These merits were missing in our current study in which the polymerization of precursors (sodium silicate and titania oxychloride) in the presence of a templating agent were done simultaneously [31]. This synthesis route was called one-pot co-condensation or direct functionalization method. Nevertheless, although the grafting method might be useful for applications where high titania loadings are desired, it has some shortcomings. First, attachment of a guest component on the pore surface reduces pore size and pore volume, which is undesirable in many cases. Second, there is little control over loading, and there is lack of stability.

The formation of finger-like structures observed in the present study (Figs. 1, 2) can be attributed to the cylindrical rearrangement of CTAB micelles above the critical micelle concentration (CMC). It has previously been reported that the CMC of CTAB is 0.03% [32]. Above this CMC, a transition from spherical micelles to rod-like micelles occurs, and the size of micelles increases with an increasing concentration of CTAB, eventually resulting in long, finger-like micelles. Despite the considerable number of studies carried out to determine the mechanism of formation of templated mesoporous silica [32–34], the actual mechanism is still unclear [35–37]. In the present work, the hydrolysis of sodium silicate by 2 N HCl resulted in the generation of sodium ions that together with the surfactant ($CTA^+$) cations acted as flocculating agents. When the initial concentration of CTAB is above its CMC, as in the present study, available charged oligomers of silica will match with the surfactant aggregates and both $Na^+$ and $CTA^+$ ions will be available as flocculating agents. In this case, small nuclei would disappear and only large particles (finger-like structures) would develop.

However, the finger-like structures observed in the present study were not very conspicuous, particularly after high temperature treatment. This indicates that the silica

framework around CTAB micelles was not very strong, resulting in the collapse of long morphologies, although some remnant fingers remained as shown in the FE-SEM micrograph in Fig. 2 (circled). Moreover, our material was not superior to composites synthesized using TEOS as a silica precursor. Despite the poor mesoporosity of the composites as evidenced by TEM and low-angle XRD (long-range mesoporous ordering; uniform mesopores not conspicuous), our composite nevertheless is suitable for most reported applications of mesoporous materials and can be synthesized economically on an industrial production scale. Moreover, we performed an additional experiment to evaluate the effect of the template, CTAB, on the structure of the final product and synthesized untemplated composite, as discussed briefly under the section "Nitrogen physisorption studies".

The Ti concentration on support surfaces of the as-synthesized sample and the samples calcined at higher temperatures (above 900 °C) fluctuated, based on the EDS results. We ascribe this to the phase separation of composite oxides ($SiO_2$ and $TiO_2$) before heat treatment or at extremely high temperatures. Upon calcination, the titanate species aggregated and homogeneous amorphous frameworks began to crystallize because of the thermodynamic metastability of $TiO_2$ during the heat treatment. Nuclei and nanocrystals of $TiO_2$ formed on the pore walls. When this occurred, phase separation also occurred and anatase $TiO_2$ nanocrystals were embedded randomly in the matrices of amorphous $TiO_2$ and $SiO_2$. As the calcination temperature increased, the phase separation continued to progress and the $TiO_2$ nanocrystals grew further. At this stage, nanosized anatase domains and nanosized $SiO_2$-rich phase domains formed. In these extreme cases, the composite samples showed non-uniform distribution of Ti and Si during EDS data collection. Nevertheless, the material calcined at 600 °C has optimum properties and a homogeneous distribution of composite components. This was confirmed by comparing the EDS and XRF results (Table 2 and the supporting information), which gave the same results at the calcination temperature of 600 °C. It should be noted that the XRF technique gives more accurate results, than the EDS, because it is based on bulk elemental analysis and has superior detection limit. EDS data collection is based on measurement of the composite constituents existing within small regions of the sample (20 $\mu$ × 20 $\mu$, in the present study; then the average value was established). Thus, a material that gives the same results for both EDS and XRF analyses should be regarded to have a homogenous (even) distribution of the composite components.

It was previously pointed out that pore size calculations to determine the mesopore size distribution can be based both on the adsorption and desorption branches of the isotherm [38]. In the presence of mesopores, capillary condensation will occur during adsorption and is preceded by a metastable fluid state ("cylindrical meniscus"), while capillary evaporation during desorption occurs via a hemispherical meniscus, separating the vapor and the capillary condensed phase. This results in hysteresis, because pores of a specific size are filled at higher pressures and emptied at lower pressures. If the material under investigation is purely mesoporous and contains non-intersecting mesopores of cylindrical geometry and similar size, the $N_2$ isotherm will be a type IV isotherm and be accompanied by a type H1 hysteresis loop, according to the IUPAC classification [28]. Both from a historical and a thermodynamic point of view, the desorption branch is most often used to derive mesopore size distributions from the isotherm [38, and references therein]. In the present study, we also chose to use the desorption branch for PSD analysis.

It has been reported that for a system characterized by the random distribution of pores and an interconnected pore system, the hysteresis loop will be of type H2 or H3 [28], and the PSD derived from the desorption branch is often much more affected by pore network effects than the adsorption branch [38]. This will result in a different behavior of the adsorption and desorption branches of the isotherm, in particular around $P/P_0 = 0.45$ (for $N_2$ at 77 K), and lead to the forced closure of the hysteresis loop. The forced closure is due to a sudden drop in the volume adsorbed along the desorption branch in the $P/P_0$ range 0.41–0.48. This phenomenon is often referred to as the tensile strength effect (TSE) [39] and has lead to erroneous reports of narrow pore size distributions at 3.8 nm (based on desorption branch) [40–43]. The TSE phenomenon was not evident in the composite materials synthesized in this study; thus, desorption branch alone was used for the determination of PSD. To avoid mistakes and erroneous conclusions, the PSD curves should be examined based on both desorption and adsorption branches for materials containing pores in the range of 3–4 nm and revealing the TSE phenomenon.

The hysteresis loops portrayed in Figs. 3 and 4 were not significantly different between TSC samples, indicating that the increase in the size of anatase $TiO_2$ nanocrystals at 900 and 1,000 °C (higher calcination temperatures), as also evidenced by XRD, did not block the pore openings. However, as the calcination temperature increased, the BET surface area and pore volume decreased gradually (Table 1). This is attributed to grain growth from the phase transformation of anatase to rutile. The threshold temperature was about 1,000 °C. After being calcined at this temperature, the BET surface area and pore volume were 231 $m^2/g$ and 0.39 $cm^3/g$, respectively, clearly indicating the significant collapse of the mesostructure. Nevertheless, the structural collapse of pure $TiO_2$ was reported to occur

at a much lower temperature [1–3], indicating that the composite has greater thermal stability than pure $TiO_2$. This is ascribed to the stabilization of the amorphous and anatase $TiO_2$ phases by the surrounding $SiO_2$ phase through the Ti–O–Si interface. At the interface, the $SiO_2$ lattice locks the Ti–O species at the interface of the $TiO_2$ domains, preventing the nucleation that is necessary for the phase transformation to rutile. Hence, greater heat is required to drive the crystallization [44].

Kumar et al. [45] investigated the microstructures of titania membranes calcined at various temperatures by high-resolution scanning electron micrograph. They found that the powders contained small anatase crystallites before the anatase to rutile transformation, but that after phase transformation, the powders had smaller anatase crystallites and larger densified rutile regions. It is thought that smaller anatase crystallites grow into larger rutile crystallites through transformation, leading to a decrease in the number of voids among anatase crystallites, which results in a decrease in surface area and pore volume after calcination at 1,000 °C.

To evaluate the impact/influence of CTAB on the porosity of the composite materials, a similar experiment was conducted in the absence of CTAB (untemplated titania–silica composite). Generally, the porosity of the final product was less than that of the templated samples, making it unsuitable for some applications where highly porous materials are required. The maximum BET surface area, average diameter of the pores, and the maximum pore volume obtained were 739 $m^2/g$, 27.4 Å, and 0.29 $cm^3/g$, respectively. This kind of product might be suitable for application in products such as paints additives and thin paper fillers.

The pore diameter of the untemplated samples is larger than the pore diameter of the composite (Table 1). This indicates that as the temperature increased, large areas of the channels were filled with large anatase nanocrystallites. As explained elsewhere in this study, this increase in grain size did not change the primary shape of the mesopores, indicating that the latter were not blocked, as suggested by the hystereses loops. Moreover, as the temperature increased, the peaks of the anatase phase became stronger and sharper. The thermodynamically favored rutile phase appeared at 1,000 °C. This indicates that the silica in the titania–silica composite can effectively prevent the transition from the anatase to the rutile phase during heat-treatment. It was previously reported that the gradual transformation of anatase phase to rutile phase for 100% $TiO_2$ occurred at a calcination temperature of 700 °C [46, 47], at which temperature the crystal grain size was found to be 34.2 nm. This strongly suggests that silica has a strong influence in our composite, inhibiting the formation of the rutile phase and the growth of the crystal grain. No additional weight loss was observed beyond 500 °C, implying that the titania–silica composite has a high thermal stability, consistent with our findings in this study.

Lastly, it should be noted that silica and titania atoms in the composite were connected by Ti–O–Si bonds, as evidenced by the vibration band at 954 $cm^{-1}$. The presence of this band confirms the presence of Si–O–Ti linkages in the titania–silica composite. The band at 470 $cm^{-1}$ can be assigned to the stretching vibrations of Ti–O bonds in Ti–O–Ti. Interestingly, the overall pattern of peaks in the TSC-2 sample was largely similar to that of the TSC-1 sample, indicating reduced structural collapse, even at higher calcination temperatures (up to 1,000 °C).

## Conclusions

We presented a versatile and reproducible approach to synthesize titania–silica composites with desirable properties from a relatively inexpensive silica precursor in this study. The resultant material had higher thermal stability (over 900 °C), optimum porosity, a homogeneous distribution of Ti in the silica matrix at a calcination temperature of 600 °C, and a higher BET surface area (above 300 $m^2/g$) than pure $TiO_2$. The rutile phase in the titania–silica composite appeared at a calcination temperature of 1,000 °C. Our new composite therefore overcomes the limitations noted for previously reported materials. Our approach can be extended to the large-scale, economic industrial production of titania–silica composites with application-specific desirable properties. Our approach can also help elucidate the pre- and post-calcination morphologies, porosity changes, and percentage composition of materials in the final product at various calcination temperatures.

**Acknowledgements** We would like to thank the Ministry of Commerce and Industries of the Republic of Korea for financial support under the R & D Innovation Fund for Small and Medium Business Administration (Project Application No. S1017370).

## References

1. Su B-L (2006) Mater Today 9(1–2):55
2. Tanaka K, Hisanaga T, Rivera AP (1993) In: Ollis DF, Al-Ekabi H (eds) Photocatalytic purification and treatment of water and air. Elsevier, Amsterdam, p 169
3. Zhang Z, Wang CC, Zakaria R, Ying J (1998) J Phys Chem B 102:10871
4. Serpone N, Lawless D, Khairutdinov R (1995) J Phys Chem 99:16655
5. Xu G, Zheng Z, Wu Y, Feng N (2009) Ceram Int 35:1
6. Tuel A, Hubert-Pfalzgraf LG (2003) J Catal 217:343
7. Hou YD, Wang XC, Wu L, Chen XF, Ding ZX, Wang XX, Fu XZ (2008) Chemosphere 72:414

8. Park JK, Kim JK, Kim HK (2007) J Mater Process Tech 186:367
9. Hayashi H, Torii K (2002) J Mater Chem 12:3671
10. Wang J, Kuhn J, Lu X (1995) J Non-Cryst Solids 186:296
11. Mitrikas G (1998) J Non-Cryst Solids 224:17
12. Tillotson TM (1998) J Non-Cryst Solids 225:358
13. Zhao L, Yu J, Cheng B (2005) J Solid State Chemistry 178:1818
14. Belhekar AA, Awate SV, Anand R (2002) Catal Commun 3:453
15. Shen SD, Tian BZ, Yu CZ, Xie SH, Zhang ZD, Tu B, Zhao DY (2003) Chem Mater 15:4046
16. Yu CZ, Yu YH, Zhao DY (2000) Chem Commun 7:575
17. Franke O, Rathousky J, Schult-Ekloff G, Starek J, Zukal A (1994) Stud Surf Sci Catal 84:77
18. Corma A, Navarro MT, Pérez-Pariente J, Sanchez F (1994) Stud Surf Sci Catal 84:69
19. Morey M, Davidason A, Stucky GD (1996) Micropor Mater 6:99
20. Nair PK, Mizukami F, Nair J, Salou M, Oosawa Y, Izutsu H, Maeda K, Okubo T (1998) Mater Res Bull 33:1495
21. Zhang YH, Reller A (2003) Mater Lett 57:4108
22. Morales JM, Latorre J, Guillem C, Porter AB, Porter DB, Amorós P (2005) Solid State Sci 7:415
23. Lee JH, Yang YS (2005) J Mater Sci 40:2843. doi:10.1007/s10853-005-2434-5
24. Shen S, Deng Y, Zhu G, Mao D, Wang Y, Wu G, Li J, Liu X, Lu G, Zhao D (2007) J Mater Sci 42:7057. doi:10.1007/s10853-007-1608-8
25. Wang HN, Yuan P, Zhou L, Guo YN, Zou J, Yu AM, Lu GQ, Yu CZ (2009) J Mater Sci 44:6484. doi:10.1007/s10853-009-3578-5
26. Berube F, Kleitz F, Kaliaguine S (2009) J Mater Sci 44:6727. doi:10.1007/s10853-009-3566-9
27. Miao L, Jin P, Kaneko K, Terai A, Gabain NN, Tanemura S (2003) Appl Surf Sci 212:255
28. Sing KSW, Everett DH, Haul RAW, Moscou L, Pierotti RA, Rouquerol J, Siemieniewska T (1985) Pure Appl Chem 57:603
29. Deng W, Bodart P, Pruski M, Shanks BH (2002) Micropor Mesopor Mater 52:169
30. Kein S, Thorimbert S, Maier WF (1996) J Catal 163:476
31. Hilonga A, Kim JK, Sarawade PB, Kim HT (in press) J Mater Sci. doi:10.1007/s10853-009-4077-4
32. Delsannti M, Moussaid A, Munch JP (1993) J Colloid Interface Sci 157:285
33. Chao MC, Lin HP, Mou CY (2004) Chem Lett 33:672
34. Firouzi A, Atef F, Oertli AG, Stucky GD, Chmelka BF (1997) J Am Chem Soc 119:3596
35. Ying JY, Mehert CP, Wong MS (1998) Angew Chem Int Ed Engl 37:82
36. Vautier-Giongo C, Pastore HO (2006) J Colloid and Interface Sci 299:874
37. Patarin J, Lebeau B, Zana R (2002) Curr Opin Colloid Interface Sci 7:107
38. Groen JC, Peffer LAA, Perez-Ramirez J (2003) Micropor Mesopor Mater 60(1–3):1
39. Burgess CVG, Everett DH (1970) J Colloid Interface Sci 33:611
40. Le Van Mao R, Denes G, Vo NTC, Lavigne JA, Le ST (1995) Mat Res Soc Proc 371:123
41. Zhang Q, Gao L, Zheng S (2001) Chem Lett 1124
42. Colon G, Hidalgo MC, Nav JA (2002) Catal Today 76:91
43. Lambert CK, Gonzalez RD (1999) J Mater Sci 34:3109. doi:10.1023/A:1004657101391
44. Larson L, Drummond CJ, Chan DYC, Grieser F (1993) J Am Chem Soc 115:11885
45. Kumar KNP, Keizer K, Burggraaf AJ (1993) J Mater Chem 3:1141
46. Yang J, Zhang J, Zhu L, Chen S, Zhang Y, Tang Y, Zhu Y, Li Y (2006) J Hazard Mater B 137:952
47. Yu JG, Yu JC, Ho WK, Leung MKP, Cheng B, Zhang GK, Zhao XJ (2003) Appl Catal A 255:309